International Journal of Innovative Computing, Information and Control
Volume **16**, Number **3**, June **2020**

ICIC International ©2020 ISSN 1349-4198
pp. **879–897**

PERSONAL IDENTIFICATION USING A DELAUNAY TRIANGLE AND OPTIC DISC RETINAL VASCULAR PATTERN

Isoon Kanjanasurat[1], Boonchana Purahong[1], Hisayuki Aoyama[2]
Chawalit Benjangkaprasert[1] and Chuchart Pintavirooj[1]

[1]Faculty of Engineering
King Mongkut's Institute of Technology Ladkrabang
Chalongkrung Road, Ladkrabang, Bangkok 10520, Thailand
pe_win99@hotmail.com; yuna001@gmail.com; {chawalit.be; chuchart.pi}@kmitl.ac.th

[2]Department of Mechanical and Intelligent Systems Engineering
University of Electro-Communications
1-5-1 Chofugaoka, Chofu, Tokyo 182-8585, Japan
aoyama@mce.uec.ac.jp

Received November 2019; revised March 2020

Abstract. *Retinal vascular patterns are unique and individual. They provide highly secure and correct identity authentication. In this study, we exploit an image alignment approach based on a geometric invariant, which is the area spanned by feature-point triplets for personal identification. First, we located the optic disc by using a projection of the vascular structure in vascular extraction and extracted feature points that are bifurcations of a retinal blood vessel in the vicinity of the optic disc as the landmarks. Delaunay triangulation is then applied to the extracted feature points. The absolute invariant is then derived by taking the ratio of successive triangular area patches. The alignment is achieved by establishing correspondences between feature points after a conformal sorting step based on a derived set of absolute affine invariants. The affine transformation parameters can then be calculated by the corresponding vertices of the most robust neighbouring triangle of both inquiry and reference images. The optic disc localization results successfully located 95.95% in six widely used retinal image databases. The algorithm of vascular extraction, applied on the DRIVE database, provided an average accuracy of approximately 94.1%. The best accuracy and sensitivity for neighbouring triangle matching obtained were 99.90% and 87.66%, respectively.*
Keywords: Vessel extraction, Optic disc localization, Retinal identification, Delaunay triangle, Neighbour area ratio

1. **Introduction.** Personal authentication can be implemented in security systems using a variety of approaches, such as personal identification numbers (PINs), passwords, cards and keys [1]. Biometrics use basic physiological properties involving characteristic biological patterns of individuals, such as the face, fingerprint, iris, retina, hand geometry and DNA [2]. The significant features of these characteristics for reliable identification are the variations of selected characteristics across the human population and the uniqueness of these characteristics for each individual [3]. The retina is the most suitable target with respect to these attributes.

The retina contains many blood vessels, the patterns of which in each retina are unique, complex and complicated to modify without surgery [4]. Retinal blood vessel patterns have a high entropy in their structure [5]; even identical twins do not have a similar pattern

DOI: 10.24507/ijicic.16.03.879

[6]. This feature is what makes them unique. Thus, retinal blood vessel recognition is one of the most accurate and reliable human identification techniques.

Prior research efforts regarding retinal image identification have only confirmed that this area remains a challenging problem [7]. First, the structure of the retina is a curved surface. A weak perspective of the image is made by an uncalibrated camera, with non-linear deformation potentially occurring. Second, image overlap may be small due to significant viewpoint changes between images. Third, retinal images with uneven illumination in large fields make the extraction of retinal vessels particularly difficult. Fourth, changes in both the structure and colour of the retina in diseased eyes, a process that can take substantial time to occur, may adversely affect retinal images. The effect of eye-movement can be accomplished by localizing the optic disc, a process that is always conducted by the debasement of the identification performance. In some papers, the problem of the extracted features and comparing with other images is handled, but these solutions induce time-consuming processes on the algorithm.

Regarding human identification based on retinal images, several papers are available in the literature. These works can be classified according to their methodology for the extracted features and strategies of matching and identification. We also classify the prior studies into two main groups based on method: non-vascular- and vascular-based feature extraction approaches.

The non-vascular method uses other characteristics of retinal images, such as optic disc features or image organization properties. Zahedi et al. [8] presented a retinal image processing method for human identification using Radon transform. This method located an optic disc and used the Radon transform for extracting characteristics around an optic disc. The result was tested on DRIVE and achieved 100% accuracy. However, disadvantages are a non-various dataset that has only 40 images and that this method cannot tolerate an affine transform. Chihaoui et al. [9] presented a human identification system based on detection of the optical disc ring in retinal images. There are three stages of the method: image enhancement, optical disc detection and interest ring extraction around the centre of the optical disc; the identification performance reached 99.89% on the VARIA database, and the approach was relatively easy to implement. However, this method cannot tolerate an affine transform. Human recognition based on retinal images and using a similarity function was used by Dehghani et al. [10]. The features were extracted by corner detection algorithms and a Harris algorithm. The matching process, with a similarity function being used to match the elements in a dataset and test images, was tested on DRIVE and STARE. The advantages of this algorithm are its success rate and that it uses several images. However, it lacks the perspective of images that apply tests on the same picture, and it uses a rather complicated algorithm. The typical limitations of personal identification based on non-vascular are their sensitivity to noise, eye-movement, non-uniform illumination and different illumination conditions. However, the feature extraction in these algorithms has low computational complexity.

In another group, vascular-based methods operate with vessel characteristics by extracting minutiae points from blood vessel patterns. This approach requires a correct blood vessel pattern with straight vessels only, which becomes challenging due to the appearance of lesions in retinal images. Köse and İkibaş [11] presented a personal identification system using retinal vasculature and that calculates the similarity of measurement and compares a vascular structure of a sample and stored images. This method leads to highly accurate matching. However, it cannot tolerate affine transform and involves a substantial amount of time for comparison of vascular patterns. Lajevardi et al. [12] addressed the retina verification system based on biometric graph matching, which considered an automatic retinal verification framework. The vascular skeleton could be extracted by a spatial and graphic

matching method. The advantages of this approach included the avoidance of translation, nonlinear distortion and small rotation. Nevertheless, it provided computations in a small dataset and non-statistical model. Ortega et al. [13] performed retinal verification using a feature point-based biometric pattern. It was an authentication system, and a set of feature points was expressed as landmarks in the retinal vascular tree. The advantage of this approach was its relatively low calculation time (155 milliseconds). However, it had lower dataset images and could not tolerate an affine transformation. Nazari and Pourghassem [14] introduced a novel retina-based human identification algorithm based on a geometrical shapes feature using a hierarchical structure of matching. This method used circling regions of a blood vessel, and STARE and DRIVE retinal image datasets were used for the algorithmic decisions. The results achieved an accuracy of 100%, and the average time process was 3.216 seconds. However, this method involved complicated computation. Deng et al. [15] outlined a retinal fundus image registration approach via vascular structure graph matching that detected and was represented as global correspondences between vascular bifurcations; the method showed matching images by using the iterative closest point. The advantages of this approach are threefold: global optimum solution, invariant to linear geometric transformations and dense local feature descriptors are not required. The main limitations of the proposed method are consistent vascular segments and a lack of various databases. Although they were still time consuming and sensitive to the strengthening of engaged methods to extract the thin vessels, the previously published paper of this group reached a high performance compared to the previous group of works.

In this paper, we study retinal image identification following vessel-based methods. We are motivated by the fact that a retinal image may contain some unique geometric structures within its vascular patterns. The similarity problem is not merely a one-to-one mapping issue between point sets but rather a pairwise matching problem between two separate vascular patterns. A short overview of our approach is represented in Figure 1, illustrating how the blood vessels in retinal feature extraction are analyzed at first to generate a triangle mesh. Then, graph matching-based identification is completed to accomplish both alignments of the retinal images.

There are three significant contributions of this research. First, we described that the retinal structure problem could be efficiently solved within the combination method of both invariant transformation and geometric techniques. Second, we proposed a simple algorithm for optic disc localization and blood vessel extraction. The method involves a short time calculation and provides highly accurate results. Third, we proposed neighbouring triangular ratio matching to eliminate incorrect correspondences from matching results.

This paper is organized as follows. Blood vessel extraction is shown in Section 2.1. The optic disc localization algorithm is presented in Section 2.2. The triangular matching method is thoroughly discussed in Section 2.3. Results are provided in Section 3. A discussion and conclusion are given in Sections 4 and 5, respectively.

2. **Methodology.** This section presents the feature extraction methods used in our retinal identification algorithm, including blood vessel extraction and optic disc localization. The technique described is simple, rapid and highly accurate. A detailed process of the above two algorithms is illustrated in Figure 1. There are three steps of retina identification (Figure 1). First, blood vessel extraction is a process for acquiring a blood vessel from a retinal image by using a convolutional matrix. Second, optic disc localization involves using blood vessels and the intensity of light around the optic disc in order for it to function as a reference point. Third, triangular matching chooses the strongest triangular

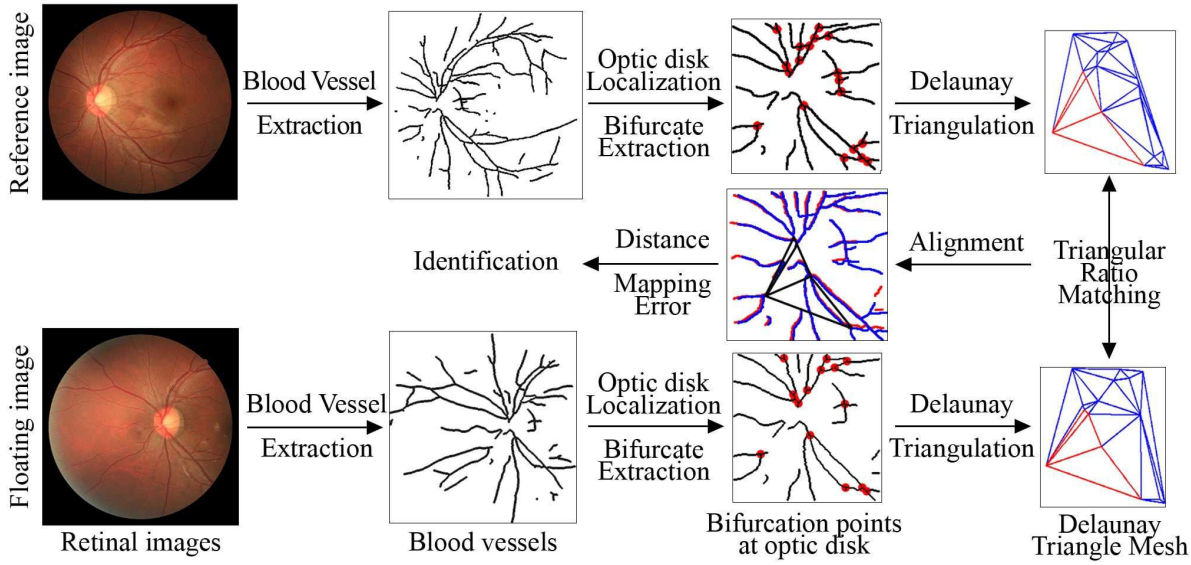

FIGURE 1. Hierarchical retinal image feature extraction and identification algorithm proposed in this paper. From left to right is the process of feature extraction, including blood vessel extraction, optic disc localization, vascular bifurcations extraction and triangular mesh representation. From right to left represents the two-step identification procedure, consisting of triangular ratio matching and distance mapping error.

mesh for transformation parameter calculation, and a similarity of pair retinal image by distance mapping error is used.

2.1. **Blood vessel extraction.** Retinal blood vessels are the most unique and apparent anatomical structures in the retina [16]. Various methods have been introduced for retinal vessel extraction, such as multiscale-based techniques [17], mathematical morphological methods [18], matched filtering approaches [19], neural network-based procedures [20], vessel tracking or tracing-based methodologies [21] and model-based techniques [22].

The proposed method uses mathematical morphological methods. Our blood vessel extraction algorithm modifies the convolutional matrix from the ultrafast optic disc localization using projection of image features [23] to increase the ability not only to locate the optic disc but also to extract the retinal blood vessels. Our technique comprises two phases. In the first phase, the proposed framework performs pre-processing to extract the vertical and horizontal edges of the blood vessel. In the second phase, the method combines vertical and horizontal edges of the blood vessel, and some morphological operations are used to reduce small isolated pixels.

In the first phase, the retinal image in Figure 2(a), which is an original retinal image, is initially resized to a height of 565 pixels, and the width of the image has a maintained aspect ratio. Second, the green channel of the retinal image is chosen for blood vessel extraction. The blood vessel in the green channel has high luminance compared to both red and blue channels. Then, the noise in the green channel is removed by a Gaussian filter, as illustrated in Figure 2(b). After that, a contrast-limited adaptive histogram equalizer (CLAHE) is used to improve the contrast of the blood vessel and reduce noise amplification (Figure 2(c)). Finally, the vertical edges (VE) in Figure 2(d) are created by using the convolution matrix A in Equation (1) with the input image, and the horizontal edges (HE) in Figure 2(e) are created by using the convolution of a transpose of matrix A with the input image. Both vertical and horizontal vessel edges were used in the next

step to create a blood vessel and locate the optic disc.

$$A = \begin{bmatrix} 1 & 0 & -1 & -1 & 0 & 1 \\ 1 & 0 & -1 & -1 & 0 & 1 \\ 1 & 0 & -1 & -1 & 0 & 1 \\ 1 & 0 & -1 & -1 & 0 & 1 \\ 1 & 0 & -1 & -1 & 0 & 1 \\ 1 & 0 & -1 & -1 & 0 & 1 \end{bmatrix} \tag{1}$$

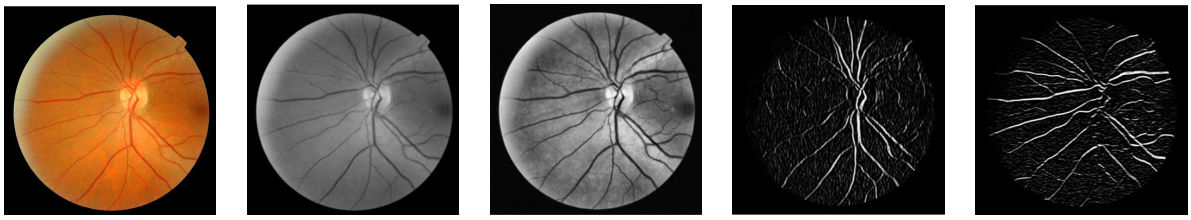

(a) (b) (c) (d) (e)

FIGURE 2. Output images at different stages in the first phase: a) original, b) green channel with Gaussian filter, c) CLAHE, d) vertical edges, and e) horizontal edges

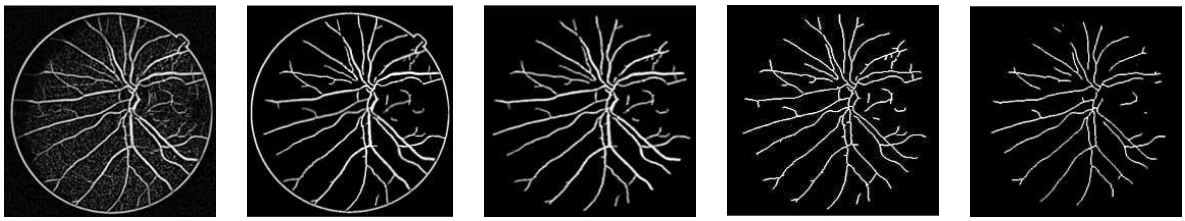

(a) (b) (c) (d) (e)

FIGURE 3. Output images at different stages in the second phase: a) combination of vertical and horizontal edge image, (b) thresholding, (c) binary image with mask, (d) skeleton of retinal blood vessel without cleaning, and (e) skeleton of retinal blood vessel with cleaning

In the second phase, the process of vascular extraction used a combination of vertical and horizontal vessel edges (as shown in Figure 3(a)) created by matrix A. It had been converted to a binary image by using the Otsu thresholding method. Small objects in a binary image were removed by morphological operations (Figure 3(b)). The circular boundary of a binary image was removed by using the mask with an AND operation (Figure 3(c)). Then, the skeleton of the retinal blood vessel in Figure 3(d) was created by the skeletonization process, involving the deletion of a boundary object without changing the essential structure of the object. The skeleton of the retinal blood vessel in Figure 3(e) has many small branches. It makes the matching process relatively time consuming. Finally, small branches in the vascular skeleton were removed by the pruning algorithm, which is a technique used in digital image processing based on mathematical morphology to remove unwanted parasitic components (spurs).

2.2. **Optic disc localization.** One particularly important characteristic of the optic disc is that it is brighter than the surrounding area [24]. Another essential feature of this disc is the origin of the retinal blood vessel; branches of the blood vessel have both vertical and horizontal directions [25]. Previous methods used optic disc localization, such as thresholding [26], a clustering-based approach [27], support-vector machine (SVM) [28], neuron network [29] and hybrid [30].

Our optic disc localization method modifies a mathematical operation from the ultrafast optic disc localization using projection of image features, as mentioned previously. There are two steps for the optic disc localization. In the first step, the horizontal optic disc position is calculated by using the ratio of vertical blood vessel edge and light intensity. In the second step, the vertical optic disc position is located by using a product of horizontal blood vessel edge and light intensity. Details regarding each step are addressed in the next section.

In the first step, the horizontal position of the optic disc is defined by the maximum ratio of the summation of vertical vessel edges and the summation of light intensity value in the sliding window. A sliding window is considered, the width of which is equal to 10% of the input image, and the height is the same as the image height. The algorithm for locating a horizontal position in Figure 4 is described below.

1) Calculate: Edgediff_Vertical = Vertical edges (VE) − Horizontal edges (HE)
2) Slide window from left to right and each step of moving calculated on Edgediff_Vertical image
   (a) SumVerEdg = a summation of vertical edges in sliding window
   (b) SumIntVal = a summation of light intensity value in sliding window
   (c) Ratio_x = SumVerEdg/SumIntVal
3) Find maximum value of Ratio_x, which it is the position of the optic disc in the horizontal axis

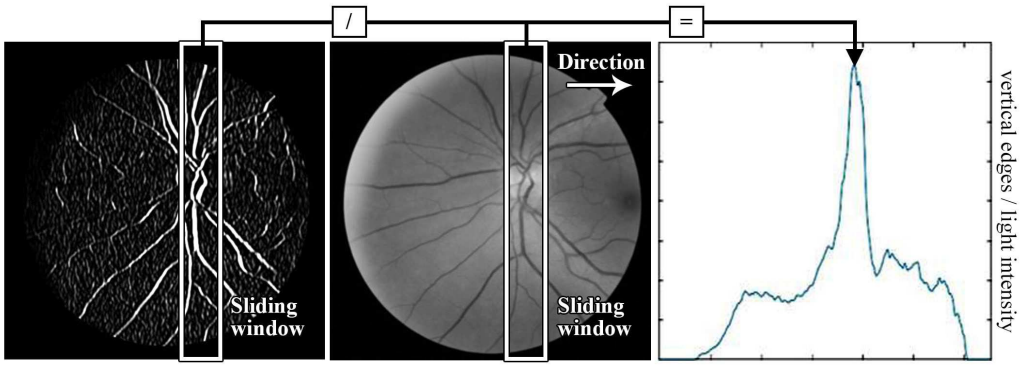

FIGURE 4. Optic disc horizontal localization process

In the second step, the vertical position of the optic disc is defined by the maximum product of the summation of horizontal vessel edges and the summation of light intensity value in the sliding window. Consider a sliding window, the width and height of which are equal to 10% of the input image. The algorithm for locating a vertical position in Figure 5 is described below.

1) Calculate: Edgediff_Horizaontal = Horizontal edges (HE) − Vertical edges (VE)
2) Slide window from left to right and each step of moving calculated on Edgediff_Horizontal image
   (a) SumHorEdg = a summation of horizontal edges in sliding window
   (b) SumIntVal = a summation of light intensity value in sliding window

(c) Ratio_y = SumHorEdg * SumIntVal

3) Find maximum value of Ratio_y, which it is the position of the optic disc in the vertical axis

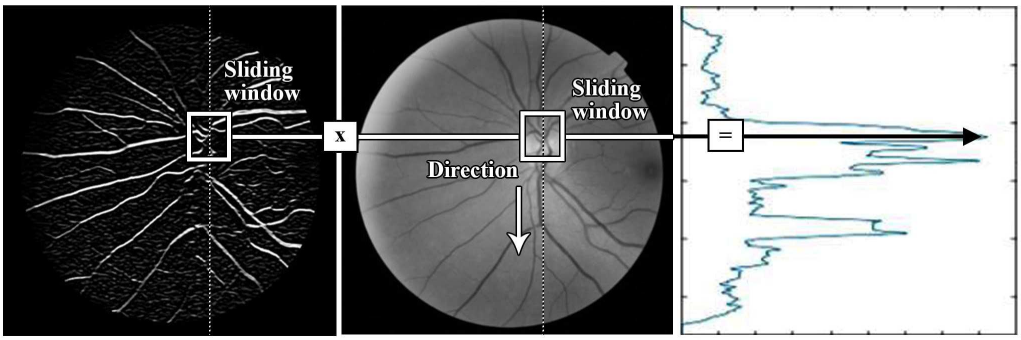

FIGURE 5. Optic disc vertical localization process

2.3. **Triangular matching.** A Delaunay triangle involves creating a triangular mesh using a set of scattered points [31]. There are four geometric characteristics of the Delaunay triangle. First, the affine invariant is a similar mesh to the original triangular mesh [32]. Second, the uniqueness of the Delaunay triangle is that adding, removing and translating points within a set of scattering affects the triangular mesh [33]. Third, this approach has noise resistance, and disrupting a vertex does not significantly change the shape of the triangular mesh. Finally, the Delaunay triangulation contains properties of local shape controllability [34] (i.e., local deformation is locally contained). The method can deal with a missing part or noise in the optic disc identification. Hence, this technique has attractive features and suitability for triangular matching. The construction of the Delaunay triangulation is shown in Figure 6.

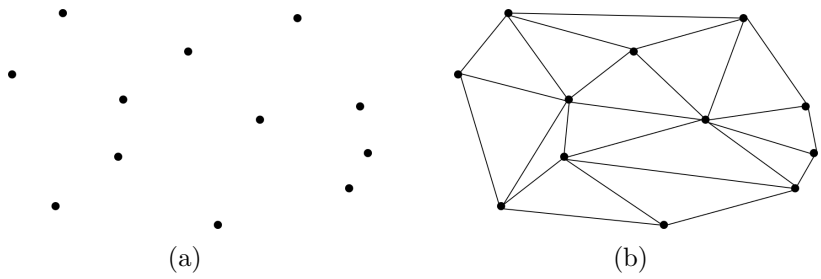

FIGURE 6. Construction of Delaunay triangulations: a) scattering, b) triangular mesh

The definition of a neighbour triangle is that it has two triangles [35], with one common edge. A part of the triangular mesh has a neighbouring triangle from 1 to 3. For example, Triangle T4 in Figure 7 has three neighbours: T1, T3 and T5. Triangle T2 has two neighbouring triangles – T1 and T3, and T5 has one neighbouring triangle (T4).

Figure 8 shows a diagram of the triangular mesh matching process, both a triangular mesh of the reference retina and another triangular mesh of a floating retina, which was created from bifurcation points in retinal vessels, which were classified by type of neighbour triangle. Then, the ratio of the area of the neighbour triangle was calculated for sorting by ascending order. After that, both reference and floating area ratios were compared one by one to find an error. A set of points in a triangular mesh, the candidate

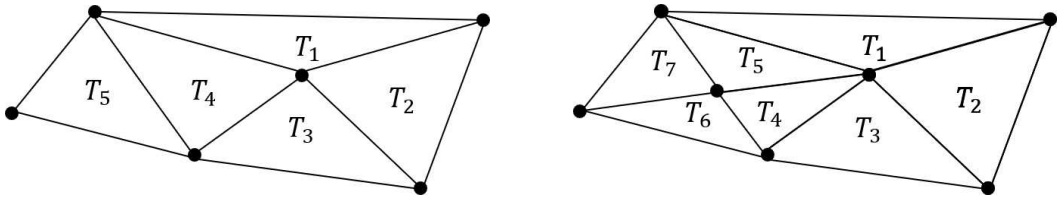

FIGURE 7. A Delaunay triangular mesh in the local area: a) original Delaunay triangular mesh, b) Delaunay triangular mesh with a point added

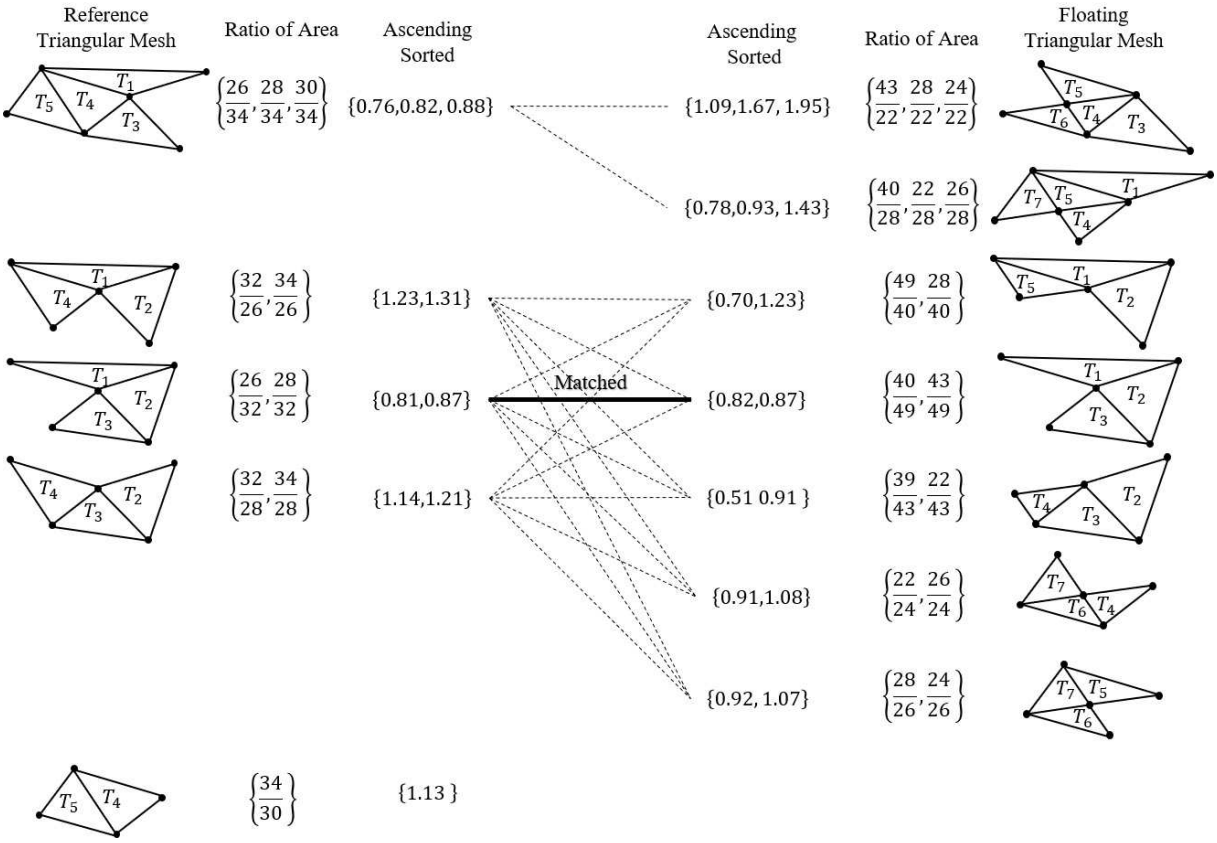

FIGURE 8. Matching neighbour triangle process

points of which are defined by points of an error ratio less than a threshold, was set for the transformation matrix calculation [36]. Finally, the matrix was estimated by the least square from the standard equation, as shown in Equation (2).

$$T = \left(Y^T Y\right)^{-1} \left(Y^T X\right) \tag{2}$$

where

$$X = \begin{bmatrix} x_1 & y_1 & 1 \\ x_2 & y_2 & 1 \\ \vdots & \vdots & \vdots \\ x_m & y_m & 1 \end{bmatrix} \quad Y = \begin{bmatrix} x'_1 & y'_1 & 1 \\ x'_2 & y'_2 & 1 \\ \vdots & \vdots & \vdots \\ x'_m & y'_m & 1 \end{bmatrix} \tag{3}$$

x and y are the set of the candidate bifurcation points in reference images and inquiry images, respectively.

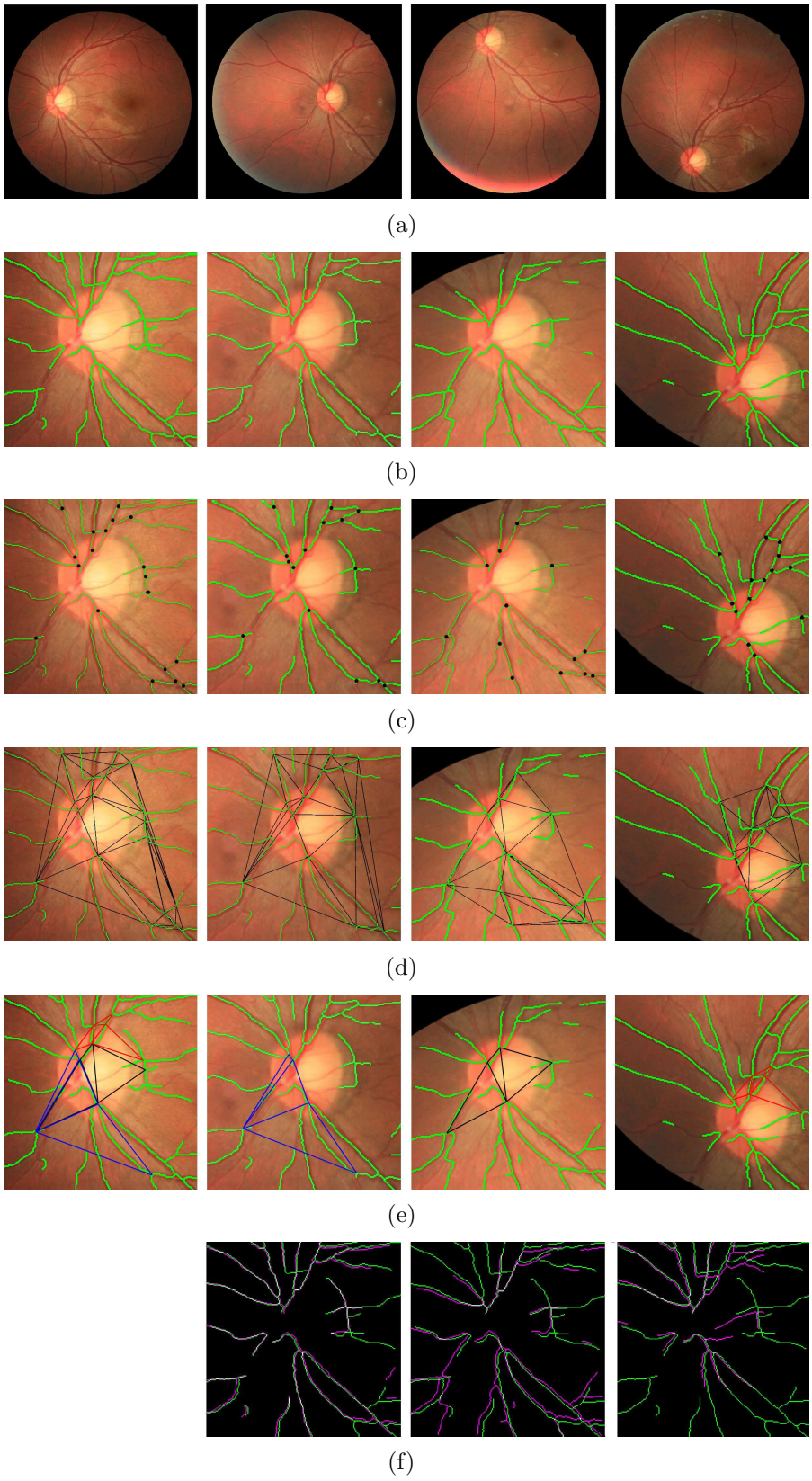

FIGURE 9. (color online) Matching process: a) optic disc from the same person, b) skeleton of optic disc, c) bifurcation of skeleton, d) Delaunay triangular mesh, e) match neighbour triangle, and f) comparison of distance mapping error

The vascular skeleton of both reference and floating retinal images, obtained from the same person at different angles (Figure 9(a)), was extracted by a vascular extraction, as illustrated in Figure 9(b). Then, bifurcations of the vascular skeleton at the optic disc in Figure 9(c) were used to create a triangular mesh by using the Delaunay triangle (Figure 9(d)). The ratio of the area of the neighbour triangle was calculated and compared to find the candidate points. The transformation parameter was also calculated by the candidate points of the triangle, which passed a triangular matching process in Figure 9(e). The mapping image in Figure 9(f) was mapped by the transformation parameter and calculated an error. Finally, the value of the distance mapping error was used to decide the similarity of retinal images. The green line in Figure 9(f) is a vascular skeleton of a reference image, and the purple line is a vascular skeleton of a floating image that was mapped by the transformation parameter. The white line is formed by overlapping both green and purple lines. The error of the mapping with the transformation parameter was calculated by the distance mapping error, which indicates the distance between any point in the original space and the closest point on the transformation image. Thus, two optic discs in a similar eye have a distance mapping error close to zero. In addition, a comparison of the optic disc from the same person but another side of the eye of another person has a large distance mapping error.

3. **Experimental Results.**

3.1. **Material.** The proposed system was evaluated using six public databases: DRIVE [37,38], DIARETDB0 [39], DIARETDB1 [40], E-OPHTHA [41], FIRE [42] and RODREP [43]. DRIVE comprises 40 retinal images and size is 565×584 pixels. There are 33 normal retinal images, and 7 retinal images show signs of mild early diabetic retinopathy. The DIARETDB0 database includes 130 retinal images, 20 of which are normal and 110 containing signs of diabetic retinopathy – the image size is 1000×1152 pixels. DIARETDB1 includes 89 images, and each image has a size of 1000×1153 pixels. There are 5 normal retinal images and 84 retinal images that show signs of mild diabetic retinopathy. E-OPHTHA comprises 148 images with microaneurysms or small haemorrhages, 77 pairs of eyes and with each image having a size of 2544×2696 pixels. FIRE has 129 images; 31 pairs of eyes are split into three different categories depending on their characteristics, and their size is 2544×2696 pixels. Finally, RODREP has 1120 images and consists of 119 eyes of 70 patients with diabetic retinopathy, and the size of each image is 2000×2312 pixels. All results were obtained using Windows 10. The programming environment was MATLAB 2018a. The CPU primary frequency was 2.9 GHz, with 8 GB of memory.

3.2. **Vessel extraction.** The proposed vessel extraction's performance is validated by using three performance measures: accuracy, specificity and sensitivity [44,45]. Four parameters referred to the classification. True positive (TP) is the number of pixels that are correctly classified as a vessel. False positive (FP) indicates the number of non-vessels that are incorrectly classified as a vessel. True negative (TN) is the number of non-vessels or background, with the correct type being identified. Finally, false negative (FN) indicates the number of pixels that were vessels but classified as non-vessels. Accuracy (ACC) is the ability of the method to differentiate a vessel and background correctly. It is calculated by determining the proportion of TP and TN. Mathematically, this can be stated as Equation (4).

$$\text{Accuracy} = \frac{(\text{TP} + \text{TN})}{(\text{TP} + \text{FP} + \text{TN} + \text{FN})} \tag{4}$$

Specificity (SP) is defined in this case as the ability to determine the background correctly. It is calculated by the proportion of TN. Mathematically, this can be stated as Equation (5).

$$\text{Specificity} = \frac{\text{TN}}{(\text{TN} + \text{FP})} \tag{5}$$

Sensitivity (SE) involves the ability to determine the vessel correctly and is calculated by the proportion of TP. Mathematically, this can be stated as Equation (6).

$$\text{Sensitivity} = \frac{\text{TP}}{(\text{TP} + \text{FN})} \tag{6}$$

Some results of the retinal blood vessel extraction are shown in Figure 10. A comparison of the performance in the vascular extraction on the DRIVE database with other techniques is presented in Table 1. The proposed method achieved an accuracy of 94.1%, which is above average. Specificity and sensitivity were 95.9% and 75.2%, respectively. Further, the blood vessels from the vascular extraction were sufficient for the triangular matching.

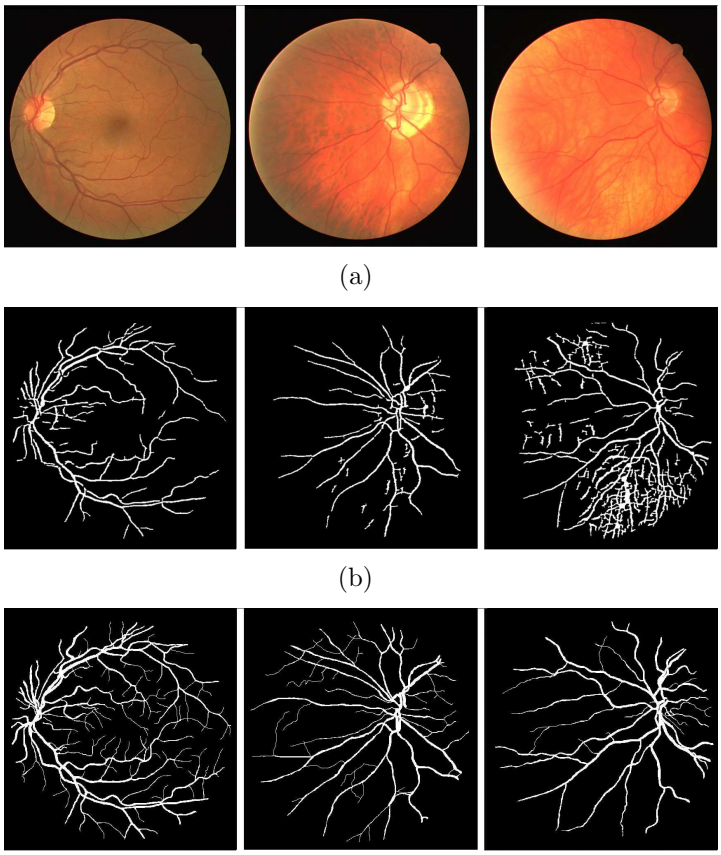

(a)

(b)

(c)

FIGURE 10. Some results of blood vessel extraction on DRIVE databases: a) original images, b) results of extraction, and c) ground truth

3.3. **Optic disc localization.** The performance of the proposed method for optic disc localization was determined for all six databases. Then, the success rate was computed for each database individually, as shown in Equation (7).

$$\text{successful rate} = \frac{\text{total number of correctly identified OD}}{\text{total images}} \tag{7}$$

TABLE 1. Comparison of blood vessel extraction method with published methods on DRIVE database

Author	Year	Method	ACC	SE	SP
Liskowski and Krawiec [20]	2016	Deep neural network	0.923	0.924	0.916
Zhu et al. [46]	2016	An ensemble classification using 36-d feature vector	0.962	0.746	0.983
Farokhain et al. [47]	2017	Gabor filter and parameter optimization	0.939	0.693	0.979
Rad et al. [48]	2017	Morphological region-based initial contour (MRBIC)	0.961	0.696	0.972
Orlando et al. [49]	2017	Discriminatively trained fully connected conditional random field model	–	0.789	0.968
Yanhui et al. [50]	2018	Convolution neural network with reinforcement sample learning	0.908	0.899	0.928
Ahamed et al. [51]	2018	Multiscale line + hysteresis	0.959	0.742	0.980
Narkthewan and Maneerat [52]	2019	Image enhancement, scaling, morphological operator and filter	0.962	0.639	0.992
Fan et al. [53]	2019	Hierarchical image matting model	0.960	0.736	0.981
Dash and Senapati [54]	2020	DWT + Tyler Coye	0.949	0.731	0.989
Proposed method			0.941	0.959	0.752

The calculation of success rate for optic disc localization is based on ground truth marked by human experts. Table 2 shows a performance evaluation of the proposed system for the entire database used here.

The results of optic disc localization considered the correct location inside the actual boundary of the optic disc. The algorithm of such localization could be located in the position of an optic disc with an average accuracy of 95.59% and achieved an accuracy of 100% for DRIVE. DIARETDB0 and DIARETDB1, both of which are databases that use a diabetes retinal image, could be located 96.15% and 98.87%, respectively. E-OPHTHA, FIRE and RODREP, which are used for triangular matching, reached an accuracy 97.4%, 97.7% and 93.7%, respectively. Table 3 shows the overall performance of the proposed system compared with the state-of-the-art methods in terms of success rate. The average running time was 0.26 seconds per image. Figure 11 gives some results of the successful optic disc localization in these six databases, with the optic disc centre being highlighted with a green point.

3.4. **Triangular matching.** The performance of the neighbour triangular matching approach was good when using parameters such as vascular extraction. However, the meaning of accuracy, specificity and sensitivity had been changed. In matching, accuracy is the method's ability to identify one person from another correctly. Specificity is its ability to identify another person correctly. Sensitivity involves the ability to identify a person correctly. TP is the number of times the same person is correctly classified. FP indicates the number of times someone was classified as the same person, whereas TN is the number of times different people were correctly classified. FN indicates the number of times the same person was classified as a different person. The results of the triangular matching by using a ratio of the neighbour area were decided by the distance mapping error, which is a distance between two points [61]. Figure 12 shows some mapping images with the transformation equation. Optic discs R1 and I1 in Figure 11 are similar but

TABLE 2. Comparison of optic disc localization method with published methods on DRIVE database

Author	Year	Method	Database	Success Rate (%)
Bharkad [55]	2017	Morphological dilation and median filtering operation	DRIVE	100
			DIARETDB0	96.92
			DIARETDB1	98.98
Panda et al. [25]	2017	Vessel symmetry line	DRIVE	100
			DIARETDB0	96.92
			DIARETDB1	100
			E-OPHTHA	100
Gui et al. [56]	2018	Corner detection method	DRIVE	100
Jois et al. [57]	2018	Particle swarm optimization	DRIVE	100
			DIARETDB0	96.15
			DIARETDB1	98.87
Dietter et al. [58]	2019	Vessel orientation and brightness and modify a score function	DRIVE	100
			DIARETDB0	97.8
			DIARETDB1	98.8
Ünver et al. [59]	2019	Statistical edge detection and circular Hough transform	DRIVE	100
			DIARETDB0	96.92
			DIARETDB1	98.88
Oza et al. [60]	2019	Multiscale low-rank image decomposition	DRIVE	100
			DIARETDB0	96.15
			DIARETDB1	97.75
Proposed method			DRIVE	100
			DIARETDB0	96.15
			DIARETDB1	98.87
			E-OPHTHA	97.4
			FIRE	97.7
			RODREP	93.7

with a different perspective. The error of R1 and I1 is less than R1 and I2 or R1 and I3. The triangular mesh of similar optic discs in different angled images had an error close to zero, with a maximum of overlapping between reference and inquiry skeletons. Although the triangle meshes had a ratio of the neighbouring area less than the threshold, different retinal images had significant or indeterminable errors. Table 3 shows a performance evaluation of the proposed system for the entire database used here.

The performances of the triangular matching on E-OPHTHA, FIRE and RODREP, all of which combined 227 reference retinal images and 1484 inquiry images, were divided into three parts. The first production is the 3-neighbour area ratio – it having an average accuracy of 99.90%. However, the sensitivity was 80.62%, as shown in Table 4. The average time of matching was 0.06 second per image. Next, the average accuracy of the 2-neighbour area ratio in Table 5 was found to be less than the 3-neighbour one, at 0.16%. Further, the sensitivity was increased to 83.76%. However, the computation time was increased to 0.38 second per image. The last example is the 1-neighbour area ratio. The performance in Table 6 can be seen to have an accuracy of 98.97%. Sensitivity was increased to 87.66%. However, the time of calculation was 1.64 second per image.

TABLE 3. Comparison of retinal identification method with published methods on DRIVE database

Author	Method	Database	Success Rate (%)
Waheed et al. [2]	Vascular and non-vascular retinal features	DRIVE	100
		STARE	100
Nazari and Pourghassem [14]	Circling regions of a blood vessel	DRIVE	100
		STARE	100
Köse and İkibaş [11]	Retinal vascular network	Own	99.5
Deng et al. [15]	Graph matching iterative closest point Delaunay triangulation graph	Own	100
		Own	75
Aleem et al. [62]	Retinal vascular network	DRIVE	100
		STARE	100
Sadikoglu and Üzelaltınbulat [63]	Neural network	DRIVE	97.5
Roy and Biswas [64]	Angle of any bifurcation point	DRIVE	100
		STARE	100
Proposed Method		DRIVE	100
		DIARETDB0	100
		DIARETDB1	100

4. **Discussion.** Retinal blood vessel identification systems are stable and suitable for biometric systems. One of the main goals of this experiment was to attempt to identify a person by using retinal vascular patterns with the Delaunay triangle. Our algorithm demonstrated excellent ability not only to locate the optic disc but also to extract blood vessels of retinal images. These results – optic disc localization, vascular extraction and triangular matching – achieved high performance and short time calculation.

In some works, the vessel segmentation has been applied to providing a more efficient identification with an improved success rate for the algorithm. For example, Waheed et al. [2] used retinal vascular features. They achieved a success rate of 100% both for DRIVE and STARE. Aleem et al. [62] studied retinal identification by using the retinal vascular network and reached a success rate of 100% for DRIVE and STARE.

In some studies, Delaunay triangulation has been adopted to tolerate an affine invariant that affine transformation consists of translation, scaling, rotation and shearing. Wang and He [35] proposed a matching method with images captured under affine transformation conditions. The results demonstrated excellent matching. Chuchart et al. [32] studied fingerprint alignment based on local features combined with affine geometric invariants. The approach found correspondences between the minutia points on the two different perspectives of fingerprint images. The results of this method could be used to find the corresponding minutiae and align any fingerprints in a case considered as the affine transformation.

5. **Conclusion.** The identification based on using geometric invariance, which is the area spanned by feature points extracted from the bifurcation of the vascular pattern in the vicinity of the optic disc, is proposed. After sorting the extracted area in a conformal order, the feature point correspondence is well established. The affine transformation parameters, including scale, rotation, translation and shear, are estimated. The query and retinal reference image can then be aligned. The similarity criterion is then calculated

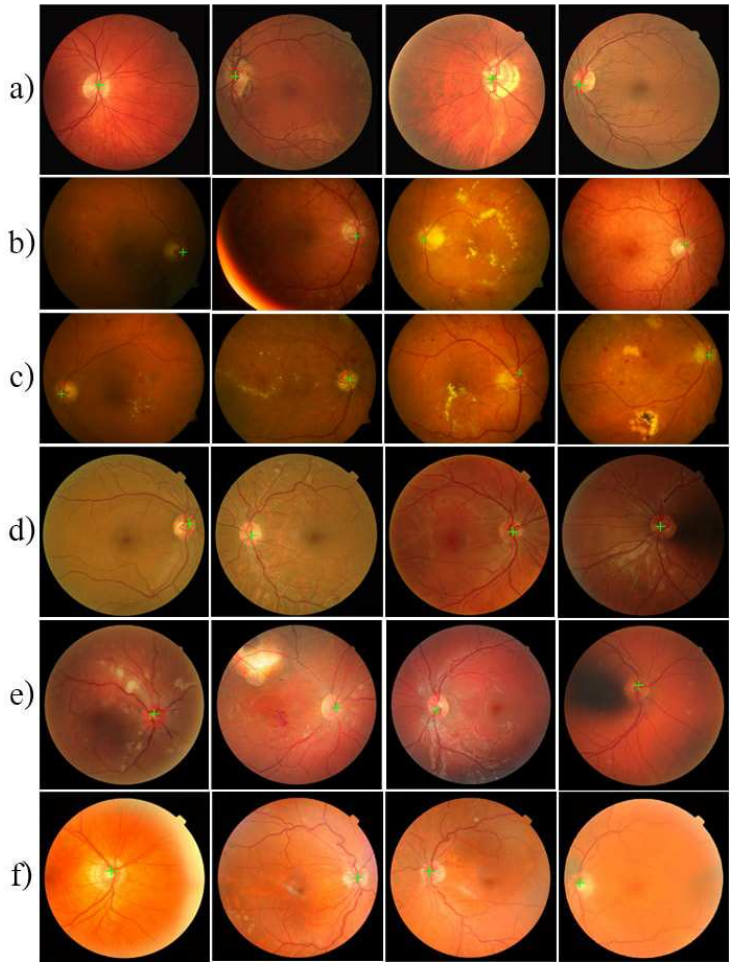

FIGURE 11. (color online) Some results of successful optic disc localizations in the six databases: a) results in DRIVE, b) results in DIARETB0, c) results in DIARETB1, d) results in E-OPHTHA, e) results in FIRE, and f) results in RODREP

and used for personal identification. The proposed methods were divided into three parts. First, optic disc localization used a characteristic of vascular patterns. It could achieve an accuracy of 95.56% and short calculation time. However, the algorithm was unable to specify the exact centre of the optic disc and did not detect optic discs located on the edge of an image. Second, vascular extraction used a combination image of a vertical vessel and horizontal vessel. The results were compared with the standard, and an accuracy of vessel extraction of more than 90% was achieved. The algorithm can detect the main blood vessel, but the small blood vessel cannot be identified. The last process – triangular matching – used the neighbouring triangular ratio to calculate transformation parameters and used the distance mapping error to verify the similarity of an optic disc. It provided an average accuracy of more than 98%. The 3-neighbour area ratio performed well with respect to time. Whereas 1-neighbour had the best accuracy, it trades off between time and efficiency. Although the research problem proposed the application of retinal image registration for person identification, the application can be more feasible for personal verification when the aim is to check the true identity of the suspected person. Another possible real-world application is to use the proposed algorithm to evaluate the healing process of the retinal lesion. For diabetes patients, for example, the retinal image shows evidence of a microaneurysm blot and flame haemorrhage, which is the leading causes of

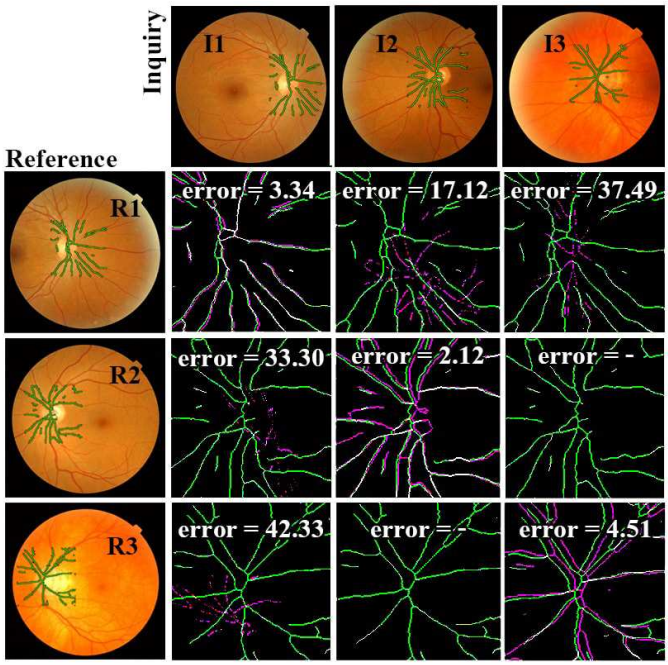

FIGURE 12. Some results of triangular matching and distance mapping error. R1 and I1 are the same eyes but from different perspectives. R2 and I2, R3 and I3 are the same eyes from different perspectives and luminance.

TABLE 4. A performance of 3-neighbour area ratio

Database	Accuracy (%)	Specificity (%)	Sensitivity (%)
E-OPHTHA	99.46	100	58.44
FIRE	99.69	100	90.32
RODREP	99.92	99.9	92.44
Overall	99.90	99.9	80.62

TABLE 5. A performance of 2-neighbour area ratio

Database	Accuracy (%)	Specificity (%)	Sensitivity (%)
E-OPHTHA	99.31	99.76	64.94
FIRE	99.58	99.78	93.55
RODREP	99.80	99.85	93.28
Overall	99.74	99.81	83.76

TABLE 6. A performance of 1-neighbour area ratio

Database	Accuracy (%)	Specificity (%)	Sensitivity (%)
E-OPHTHA	98.05	98.36	72.73
FIRE	98.15	98.82	96.77
RODREP	99.36	99.39	95.80
Overall	98.97	99.02	87.66

blindness. After medical treatment, the doctor wishes to evaluate the efficiency of the treatment. To do so, the retinal image before and after the treatment will be aligned using the proposed algorithm. Differences in the images can then be used as criteria for treatment efficiency.

REFERENCES

[1] R. Clodfelter, Biometric technology in retailing: Will consumers accept fingerprint authentication?, *Journal of Retailing and Consumer Services*, vol.17, pp.181-188, 2010.

[2] Z. Waheed, M. Usman Akram, A. Waheed, M. A. Khan, A. Shaukat and M. Ishaq, Person identification using vascular and non-vascular retinal features, *Computers & Electrical Engineering*, vol.53, pp.359-371, 2016.

[3] R. H. Abiyev and K. I. Kilic, Robust feature extraction and iris recognition for biometric personal identification, *Biometric Systems*, 2011.

[4] K. A. Toh and A. B. J. Teoh, Vascular patterns, *Encyclopedia of Cryptography and Security*, pp.1353-1356, 2011.

[5] A. Arathi, J. S. Culpepper, J. Jeffers, A. Turpin, S. Boztas, K. J. Horadam and A. M. Mckendrick, Entropy of the retina template, in *Lecture Notes in Computer Science*, M. Tistarelli and M. S. Nixon (eds.), Springer, 2009.

[6] S. Fahreddin and U. Selin, Biometric retina identification based on neural network, *Procedia Computer Science*, vol.102, pp.26-33, 2016.

[7] A. Can, C. V. Stewart, B. Roysam and H. L. Tanenbaum, A feature-based, robust, hierarchical algorithm for registering pairs of images of the curved human retina, *IEEE Trans. Pattern Analysis and Machine Intelligence*, vol.24, pp.347-364, 2002.

[8] A. Zahedi, H. Sadjedi and A. Behrad, A new retinal image processing method for human identification using Radon transform, *Iranian Conference on Machine Vision and Image Processing*, pp.1-4, 2010.

[9] T. Chihaoui, R. Kachouri, H. Jlassi, M. Akil and K. Hamrouni, Human identification system based on the detection of optical disc ring in retinal images, *International Conference on Image Processing Theory*, pp.263-267, 2015.

[10] A. Dehghani, Z. Ghassabi, H. A. Moghddam and M. S. Moin, Human recognition based on retinal images and using new similarity function, *EURASIP Journal on Image and Video Processing*, vol.58, 2013.

[11] C. Köse and C. İkibaş, A personal identification system using retinal vasculature in retinal fundus images, *Expert Systems with Applications*, vol.38, pp.13670-13681, 2011.

[12] S. M. Lajevardi, A. Arakala, S. A. Davis and K. J. Horadam, Retina verification system based on biometric graph matching, *IEEE Trans. Image Processing*, vol.22, pp.3625-3635, 2013.

[13] M. Ortega, M. G. Penedo, J. Rouco, N. Barreira and M. J. Carreira, Retinal verification using a feature points-based biometric pattern, *Journal on Advances in Signal Processing*, pp.1-13, 2009.

[14] P. Nazari and H. Pourghassem, A novel retina-based human identification algorithm based on geometrical shape features using a hierarchical matching structure, *Computer Methods and Programs in Biomedicine*, vol.141, pp.43-58, 2017.

[15] K. Deng, J. Tian, J. Zheng, X. Zhang, X. Dai and M. Xu, Retinal fundus image registration via vascular structure graph matching, *International Journal of Biomedical Imaging*, 2010.

[16] K. B. Khan, A. A. Khaliq and A. Jalil, A review of retinal blood vessels extraction techniques: Challenges, taxonomy, and future trends, *Pattern Analysis and Applications*, pp.767-802, 2019.

[17] M. E. Martinez-Perez, A. D. Hughes, S. A. Thom, A. A. Bharath and K. H. Parker, Segmentation of blood vessels from red-free and fluorescein retinal images, *Medical Image Analysis*, pp.47-61, 2017.

[18] E. Sigursson, S. Valero, J. Benediktsson, J. Chanussot, H. Talbot and E. Stefansson, Automatic retinal vessel extraction based on directional mathematical morphology and fuzzy classification, *Pattern Recognition Letters*, vol.47, pp.164-171, 2014.

[19] N. Singh and R. Srivastava, Retinal blood vessels segmentation by using Gumbel probability distribution function based matched filter, *Computer Methods and Programs in Biomedicine*, pp.40-50, 2016.

[20] P. Liskowski and K. Krawiec, Segmenting retinal blood vessels with deep neural networks, *IEEE Trans. Medical Imaging*, vol.35, no.11, pp.2369-2380, 2016.

[21] E. Poletti and A. Ruggeri, Graph search retinal vessel tracking, *Ophthalmological Imaging and Applications*, pp.97-115, 2014.

[22] G. Kovács and A. Hajdu, A self-calibrating approach for the segmentation of retinal vessels by template matching and contour reconstruction, *Medical Image Analysis*, pp.24-46, 2016.

[23] A. E. Mahfouz and A. S. Fahmy, Ultrafast optic disc localization using projection of image features, *IEEE International Conference on Image Processing*, pp.665-668, 2009.

[24] M. U. Akram, A. Khan, K. Iqbal and W. H. Butt, Retinal images: Optic disk localization and detection, *Image Analysis and Recognition*, pp.40-49, 2010.

[25] R. Panda, N. B. Puhan and P. Ganapati, Robust and accurate optic disk localization using vessel symmetry line measure in fundus images, *Biocybernetics and Biomedical Engineering*, pp.466-476, 2017.
[26] S. Debasree and D. Soumen, Automated glaucoma detection of medicalimage using biogeography based optimization, *Proc. of Advances in Optical Science and Engineering*, pp.381-388, 2017.
[27] N. Thakur and M. Juneja, Clustering based approach for segmentation of optic cup and optic disc for detection of glaucoma, *Current Medical Imaging Reviews*, pp.99-105, 2017.
[28] S. Maheshwari, R. B. Pachori, V. Kanhangad, S. V. Bhandary and U. R. Acharya, Iterative variational mode decomposition based automated detection of glaucoma using fundus images, *Computers in Biology and Medicine*, pp.142-149, 2017.
[29] J. E. W. Koh, E. Y. K. Ng, S. V. Bhandary, A. Laude and U. R. Acharya, Automated detection of retinal health using PHOG and SURF features extracted from fundus images, *Applied Intelligence*, pp.1-15, 2017.
[30] M. P. Sarathi, M. K. Dutta, A. Singh and C. M. Travieso, Blood vessel inpainting based technique for efficient localization and segmentation of optic disc in digital fundus images, *Biomedical Signal Processing and Control*, vol.25, pp.108-117, 2016.
[31] J. Dou and J. Li, Image matching based local Delaunay triangulation and affine invariant geometric constraint, *Optik*, pp.526-531, 2014.
[32] P. Chuchart, S. C. Fernand and I. Woranut, Fingerprint alignment based on local feature combined with affine geometric invariant, *International Conference in Central Europe on Computer Graphics*, pp.173-178, 2010.
[33] G. Bebis, T. Deaconu and M. Georgiopoulos, Fingerprint identification using Delaunay triangulation, *International Conference on Information Intelligence and Systems*, pp.452-459, 1999.
[34] K. Javad and K. A. Mohammad, Fingerprint indexing based on expanded Delaunay triangulation, *Expert Systems with Applications*, pp.251-267, 2017.
[35] L. Wang and X. He, Affine image matching using Delaunay triangles, *International Conference on Estimation Detection and Information Fusion*, pp.34-39, 2015.
[36] Z. Yang and F. S. Cohen, Image registration and object recognition using affine invariants and convex hulls, *Image Processing*, pp.934-946, 1999.
[37] J. J. Staal, M. D. Abramoff, M. Niemeijer, M. A. Viergever and B. V. Ginneken, Ridge based vessel segmentation in color images of the retina, *IEEE Trans. Medical Imaging*, pp.501-509, 2004.
[38] M. Niemeijer, J. J. Staal, B. V. Ginneken, M. Loog and M. D. Abramoff, Comparative study of retinal vessel segmentation methods on a new publicly available database, *SPIE Medical Imaging*, pp.648-656, 2004.
[39] T. Kauppi, V. Kalesnykiene, J.-K. Kamarainen, L. Sorri, H. Uusitalo, H. Kälviäinen and J. Pietilä, *DIARETDB0: Evaluation Database and Methodology for Diabetic Retinopathy Algorithms*, Technical Report, 2006.
[40] T. Kauppi, V. Kalesnykiene, J.-K. Kamarainen, L. Sorri, H. Uusitalo, H. Kälviäinen and J. Pietilä, DIARETDB1 diabetic retinopathy database and evaluation protocol, *The British Machine Vision Conference*, 2007.
[41] E. Decencière, G. Cazuguel, X. Zhang, G. Thibault, J. C. Klein, F. Meyer, B. Marcotegui, G. Quellec, M. Lamard, R. Danno, D. Elie, P. Massin, Z. Viktor, A. Erginay, B. Laÿ and A. Chabouis, TeleOphta: Machine learning and image processing methods for teleophthalmology, *IRBM*, pp.196-203, 2013.
[42] C. Hernandez-Matas, X. Zabulis, A. Triantafyllou, P. Anyfanti, S. Douma and A. A. Argyros, FIRE: Fundus image registration dataset, *Journal for Modeling in Ophthalmology*, pp.16-28, 2017.
[43] K. M. Adal, P. G. Etten, J. P. Martinez, L. J. Vliet and K. A. Vermeer, Accuracy assessment of intra and inter-visit fundus image registration for diabetic retinopathy screening, *Investigative Ophthalmology & Visual Science*, pp.1805-1812, 2015.
[44] M. M. Fraz, P. Remagnino, A. Hoppe, S. Velastin, B. Uyyanonvara and S. A. Barman, A supervised method for retinal blood vessel segmentation using line strength multiscale Gabor and morphological features, *IEEE International Conference on Signal and Image Processing Applications*, pp.410-415, 2011.
[45] W. A. B. Wan Mustafa, H. Yazid, S. B. Yaacob and S. N. Bin Basah, Blood vessel extraction using morphological operation for diabetic retinopathy, *IEEE Region 10 Symposium*, pp.208-212, 2014.
[46] C. Zhu, B. Zou, Y. Xiang, J. Cui and H. Wu, An ensemble retinal vessel segmentation based on supervised learning in fundus images, *Chinese Journal of Electronics*, no.3, pp.503-511, 2016.

[47] F. Farokhain, C. Yang, H. Demirel, S. Wu and I. Beheshti, Automatic parameters selection of Gabor filters with the imperialism competitive algorithm with application to retinal vessel segmentation, *Biocybernetics & Biomedical Engineering*, vol.37, no.1, pp.246-254, 2017.

[48] A. E. Rad, M. S. M. Rahim, H. Kolivand and I. B. M. Amin, Morphological region-based initial contour algorithm for level set methods in image segmentation, *Multimedia Tools and Applications*, vol.76, pp.2185-2201, 2017.

[49] J. I. Orlando, E. Prokofyeva and M. B. Blaschko, A discriminatively trained fully connected conditional random field model for blood vessel segmentation in fundus images, *IEEE Trans. Biomedical Engineering*, vol.64, no.1, pp.16-27, 2017.

[50] G. Yanhui, B. Ümit, J. Lucas, K. Khorasani and A. Şengür, A retinal vessel detection approach using convolution neural network with reinforcement sample learning strategy, *Measurement*, pp.586-591, 2018.

[51] A. T. U. Ahamed, A. Jothish, G. Johnson and S. B. V. Krishna, Automated system for retinal vessel segmentation, *The 2nd International Conference on Inventive Communication and Computational Technologies*, pp.717-722, 2018.

[52] A. Narkthewan and N. Maneerat, Retina blood vessel detection for diabetic retinopathy diagnosis, *International Conference on Biomedical Engineering and Technology*, pp.149-152, 2019.

[53] Z. Fan, J. Lu, C. Wei, H. Huang, X. Cai and X. Chen, A hierarchical image matting model for blood vessel segmentation in fundus images, *IEEE Trans. Image Processing*, vol.28, no.5, pp.2367-2377, 2019.

[54] S. Dash and M. R. Senapati, Enhancing detection of retinal blood vessels by combined approach of DWT, Tyler Coye and Gamma correction, *Biomedical Signal Processing and Control*, 2020.

[55] S. Bharkad, Automatic segmentation of optic disk in retinal images, *Biomedical Signal Processing and Control*, pp.483-498, 2017.

[56] B. Gui, R. J. Shuai and P. Chen, Optic disc localization algorithm based on improved corner detection, *Procedia Computer Science*, pp.311-319, 2018.

[57] S. P. S. Jois, S. Harsha and J. R. H. Kumar, Automatic optic disc localization using particle swarm optimization technique, *TENCON IEEE Region 10 Conference*, pp.1718-1722, 2018.

[58] J. Dietter, W. Haq, V. I. Iliya, L. A. Norrenberg, M. Völker, M. Dynowski, D. Röck, F. Ziemssen, A. M. Leitritz and M. Ueffing, Optic disc detection in the presence of strong technical artifacts, *Biomedical Signal Processing and Control*, 2019.

[59] H. M. Ünver, Y. Kökver, E. Duman and O. A. Erdem, Statistical edge detection and circular Hough transform for optic disk localization, *Applied Sciences*, vol.9, 2019.

[60] D. Oza, A. Nair and J. R. H. Kumar, A novel application of multiscale low-rank image decomposition for optic disc localization, *TENCON IEEE Region 10 Conference*, pp.2690-2694, 2019.

[61] P. E. Danielsson, Euclidean distance mapping, *Computer Graphics and Image Processing*, pp.227-248, 1980.

[62] S. Aleem, B. Sheng, P. Li, P. Yang and D. D. Feng, Fast and accurate retinal identification system: Using retinal blood vasculature landmarks, *IEEE Trans. Industrial Informatics*, pp.4099-4110, 2019.

[63] F. Sadikoglu and S. Üzelaltınbulat, Biometric retina identification based on neural network, *Procedia Computer Science*, 2016.

[64] N. D. Roy and A. Biswas, Detection of bifurcation angles in a retinal fundus image, *The 8th International Conference on Advances in Pattern Recognition*, 2015.